Contents lists available at ScienceDirect

Composites: Part A

journal homepage: www.elsevier.com/locate/compositesa

The relationship between pure delamination modes I and II on the crack growth rate process in cracked lap shear specimen (CLS) of 5 harness satin composites

M.Y. Shiino [a,*], R.C. Alderliesten [b], M.V. Donadon [c], M.O.H. Cioffi [d]

[a] *Instituto de Ciência e Tecnologia, UNESP – Univ Estadual Paulista, Campus de São José dos Campos, Departamento de Engenharia Ambiental, Rodovia Presidente Dutra, km 137.8, 12247-004 São José dos Campos, SP, Brazil*
[b] *Faculty of Aerospace Engineering, Delft University of Technology – TUDelft, Aerospace Structures & Materials, Kluyverweg 1, 2629 HS Delft, The Netherlands*
[c] *Instituto Tecnológico da Aeronáutica – ITA, Praça Marechal do Ar Eduardo Gomes, Vila das Acácias CEP, 12228-900 São José dos Campos, SP, Brazil*
[d] *Faculdade de Engenharia de Guaratinguetá, UNESP – Univ Estadual Paulista, Departamento de Materiais e Tecnologia, Fatigue and Aeronautic Materials Research Group, Av. Dr. Ariberto Pereira da Cunha 333, 12516-410 Guaratinguetá, SP, Brazil*

ABSTRACT

Carbon fiber reinforced polymers (CFRP) structure can include dropping-off plies in order to comply with design requirements aiming at significant weight savings. However this type of discontinuity represents a potential source of delamination initiation and propagation which requires assessment of the mechanisms acting at the crack tip. This research investigates the influence of delamination modes I and II on the overall damage process observed in CLS specimen subjected to cyclic loads. The main contribution of this work focuses on the identification and physical interpretation of complex failure mechanisms in harness satin fabric. For this purpose a detailed fractographic analysis was carried out to qualitatively assess the surface fractures in these type of laminates. Results obtained for cyclic loaded CLS specimens were compared to analytical closed form solutions available in the literature. Results indicated that delamination front exhibited distinguishable delamination modes I and II propagating at constant mixed mode ratio (G_I/G_T).

© 2015 Elsevier Ltd. All rights reserved.

1. Introduction

Laminated composites processed with woven fabrics have been widely employed as structural components in a diversified field of application. Its versatility of application is explained by better balanced properties in comparison to unidirectional laminates and good drapability which avoids wrinkles when preforming the fabrics into complex mold cavities [1,2].

A concern for this type of laminate is related to the difficult interpretation or prediction of the propagation path at an irregular surface structure of fill and warp pattern in plain weave (PW) or a harness satin (HS) fabrics [3,4]. In regard to quasi-static loading, the process of delamination growth was well described in work conducted by Shiino et al. [3]. For modes I and II of a 5HS laminate [3], however for fatigue, the process of delamination involves

damage accumulation at fill pattern that was partially described by Shiino et al. [5].

Regarding this type of laminate in crack lap shear (CLS) configuration, no report has been found that describes the delamination behavior including full detail of mode interactions at the crack tip. Studies using CLS specimen configuration can be found in the open literature [6,7]. However these previous studies are either associated to unidirectional laminates or isotropic materials where closed form solution and finite element based analysis are proposed [6–8]. These results show predominantly contribution of mode II loading at the CLS crack tip although Reddy et al. [8] commented that mode I loading usually drives the delamination growth.

In relation to the type of failure in composite laminates, the event of failure depends on the laminate quality and stress intensity conditions which can be analyzed by the following failure categories: interface failure; shearing failure; matrix microcracking; and processing defects [9,10]. In general, the mode I component produces predominantly a smooth surface characterized by scarp

* Corresponding author. Tel.: +55 1239051626; fax: +55 1239479010.
  E-mail addresses: marcos.shiino@ict.unesp.br, marcosshiino@yahoo.com.br (M.Y. Shiino).

formation that represents the action of peel stresses; meanwhile, the mode II component creates a surface roughness that is interpreted as shear stress dominant failure mode [9,11,12]. The scarp fracture pattern is formed by the coalescence of riverlines also related to the plastic microcreep fracture mechanism, which grows from neighboring fibers and converges into scarps [13–15]. Besides, riverlines may also indicate the crack propagation direction [13].

For structures the behavior of the delamination is much like the CLS configuration, in which a combination of modes I, II and even III acts at the crack tip characterizing a mixed mode propagation. Consequently, the fracture morphology will be different from that in pure modes of propagation [14].

Regarding the behavior of propagation in CLS specimens, Fortson and Armanios [9] observed crack arrest in unidirectional laminates, a phenomena that normally occurs in woven fabrics [4,5]. In fact, in work conducted by Rhee and Chi [16], the fracture surface morphology presented evidences of crack migration between layers with fiber direction at 0° and 90°.

This work directly associates crack growth rate (da/dN) with fracture surfaces in pure modes I and II and associates its characteristic features with a specimen designed to develop mixed mode loading named as CLS in which its mode ratio (G_I/G_{II}) was partially solved for isotropic materials and unidirectional composites [17], sometimes using finite element analysis [18]. For this purpose, a detailed discussion on pure loading modes will be presented first before providing details on the crack interaction of modes I and II in CLS specimen, which has a simple geometry for providing mix mode of delamination [19]. The main reason for providing this qualitative information on mode ratio is the complex stress state at the crack tip that is not explained at all in the analytical approaches available in the literature.

2. Materials and methods

2.1. Materials and process

The 5HS woven fabric supplied by HEXCEL was placed in a mold with dimensions of $300 \times 400 \times 3 \, mm^3$. The woven fabric had an areal weight of 391 g/m^2, and consisted of 6 K HTA carbon fibers with its surface coated by epoxy powder in order to result in a preform with rectangular shape. The resulting laminate with 8 plies total had a final fiber volume fraction (FVF) of about 58%. A 13 µm polytetrafluoroethylene (PTFE) insert film was introduced at the middle plane of the laminate to produce an artificial pre-crack, as specified in ASTM D5528-01 [20].

The laminate was produced via resin transfer molding (RTM) using a bi-component RTM-6 epoxy resin system also supplied by HEXCEL. After the injection step, the panel was cured at a temperature of 180 °C for 120 min.

The final laminate was inspected with a through-transmission ultrasonic test (TT) with 1410 C-scan equipment.

2.2. Interlaminar fracture toughness tests

This section describes the three configurations used for fatigue tests in modes I, II and I/II as well as the procedures to calculate the energy release rate (G).

2.2.1. Mode I

Quasi-static double cantilever beam (DCB) tests were carried out in accordance with the standard test method described in ASTM 5528-01 [20] using an MTS testing machine with a 5 kN load capacity cell at room temperature. The mode I data reduction was conducted using modified beam theory (MBT). Further details of the data reduction are well outlined in [20].

The tests were carried out under a frequency of 5 Hz and a stress ratio of $R = 0.1$ with displacement control with a start point at critical displacement δ_{Ic} that is related to the critical energy release rate G_{Ic}. Before the fatigue tests a pre-crack of approximately ≈ 2 mm was conducted with a rate of 1 mm/min until the crack moved forward from the insert film to avoid any influence of the resin pocket created during the injection process.

The crack was monitored with lens of 50 mm diameter, 2.8 aperture and the images were captured every 500 cycles with Labview v.12.0 software. These images were post-processed with Image J software which was also used to measure the resulting crack increments.

The energy release rate was determined by using the relationship between the compliance $C = \delta/P$ and the crack length a, as illustrated in Fig. 1, in combination with Eq. (1).

$$G = \frac{P}{2B} \frac{dC}{da} \qquad (1)$$

where G is the strain energy release rate (SERR), B is the specimen width, C the compliance and a the crack length.

2.2.2. Mode II

For mode II fatigue tests, a specimen geometry similar to double cantilever beam was used but now loaded using a three-point-bending device. A support span was employed to be equal to $2L = 100$ mm, an initial crack length equal to $a_0 = 35$ mm, and same fatigue parameters as employed for mode I tests. The procedure for conducting the test was similar as adopted by O'Brien for unidirectional laminates [21].

The SERR value was determined using Eq. (1) in combination with the derivation of the relation between compliance and crack length: $C = A + na^3$. The determination of the slope n was based on Fig. 2.

2.2.3. Axial delamination mode

This test was conducted using specimens with a geometry that includes a discontinuity located at half of the thickness as shown in Fig. 3. The fatigue test was conducted using force control in a universal testing machine Instron 8801 with a 100 kN loading cell. The fatigue parameters followed the same as for other modes of propagation. To correlate the crack length with the change in compliance, the specimens were instrumented with strain gage. The complete setup is shown in Fig. 4.
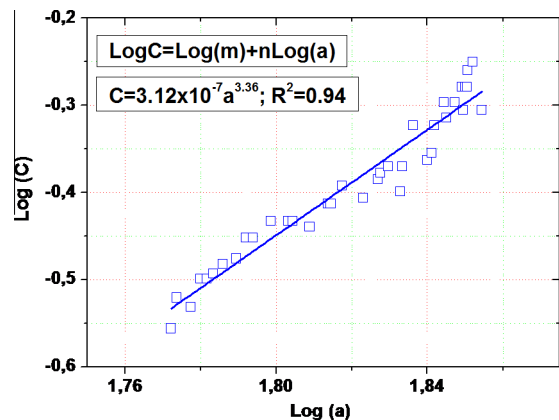

Fig. 1. Graphic for determination of the equation $C = ma^n$. (For interpretation of the references to color in this figure legend, the reader is referred to the web version of this article.)
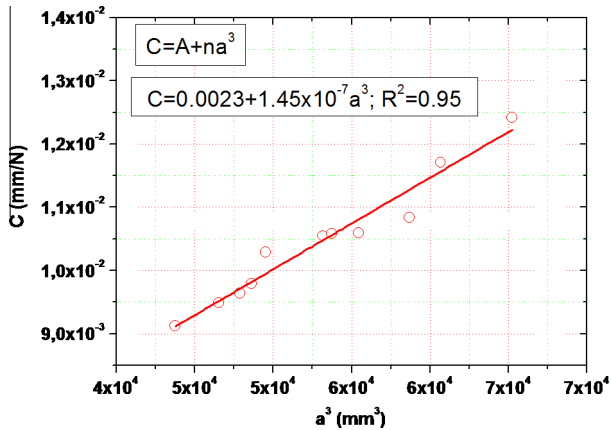
Fig. 2. Graphic for determination of the slope *n*. (For interpretation of the references to color in this figure legend, the reader is referred to the web version of this article.)

The energy involved in the crack increment was determined by using Eq. (2) which is based on the elementary equilibrium of momentum in elasto-statics [20,22].

$$G_c = \frac{P_c^2}{2b^2}\left(\frac{1}{E_s t_s} - \frac{1}{E_s t_s + E_l t_l}\right) \qquad (2)$$

where the subscript *s* means strap (continuous section), *l* means lap (interrupted section) as indicated in Fig. 3, *P* is the applied load, *b* the width of the specimen, *t* the thickness and *E* the corresponding in-plane modulus of the sections.

2.3. Fracture surface investigation

The fracture surfaces of the specimens submitted to fatigue testing were investigated in images captured with a scanning electron microscopy (SEM) named as Zeiss EVO LS-15 equipped with a tungsten filament that was set to operate at 10–20 kV and using a high vacuum mode to boost the secondary electron acquisition.
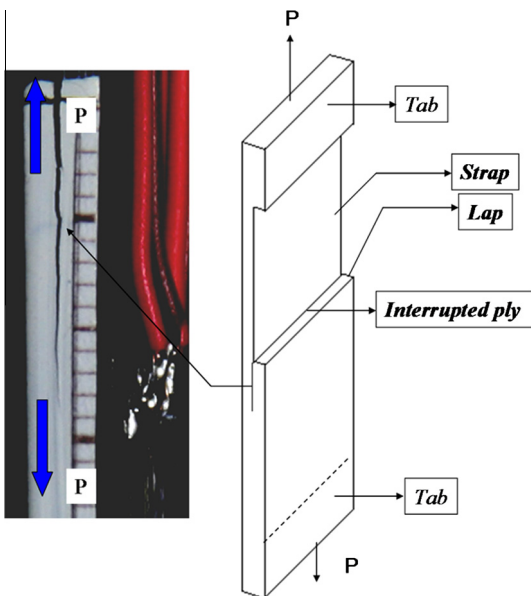

Fig. 3. Cracked lap shear (CLS) specimen. (For interpretation of the references to color in this figure legend, the reader is referred to the web version of this article.)

These parameters were chosen to prioritize the topographic information.

3. Results and discussion

3.1. Mode I – crack growth rate and fracture surface

The crack growth rate was plotted against the crack length to analyze the region of fracture surface patterns as shown in Fig. 5, where the number followed by a letter relates to the respective images (Example: 6a refers to Fig. 6a) of the fracture surfaces. The images were divided into two regions before and after the plateau limited by points 6d and 7b.

The investigation was limited to the warp sections of the 5HS fabric due to the stable and controlled manner the crack propagated, in which facilitated in tracking the crack as well as the analysis. As already discussed in [5], with the same material system (5HS/epoxy system), there is an arresting point at point 6d that creates a damage area ahead of this point, due to cyclic loading, which dictates the crack growth rate until the crack reaches another arresting point or advanced this region of non-linear behavior.

In the following fractographic analysis, the red arrow represents the global crack propagation direction and the white arrow the local crack propagation direction.

Fig. 6a corresponds to a region of higher crack growth rate similar to a specimen submitted to a quasi static loading which generated a significant amount of river markings [13] or riverlines [23] (as detailed in the orange box) that subsequently converged into scarps. This fracture section also indicates the direction of global crack propagation by taking the root of riverlines as a reference and final angle (θ) of the riverlines as depicted in Fig. 6a. The white arrow indicates an overload caused by the interlacing section (weave pattern) that formed cusp patterns that were created by mode II loading, also Greenhalgh [23] mentioned that a rotation of the main load can cause a change in the scarp formation direction which transforms into a cusp pattern. From Fig. 6b the evidence of crack propagation direction is not so well defined and the predominance of scarps indicates also peel loading. Fig. 6c also agrees with Fig. 6a in relation to the final angle of the riverlines. Just before the arresting location, the fracture surface in Fig. 6d also had riverline angles different from ϴ value and barely visible scarps which indicates a decrease in crack growth rate.

After the plateau of the *da/dN* vs *a* graphic at label 7a in Fig. 5, the curve returned to a region of constant crack growth rate, where Fig. 7a shows the very beginning of this point of scarps with
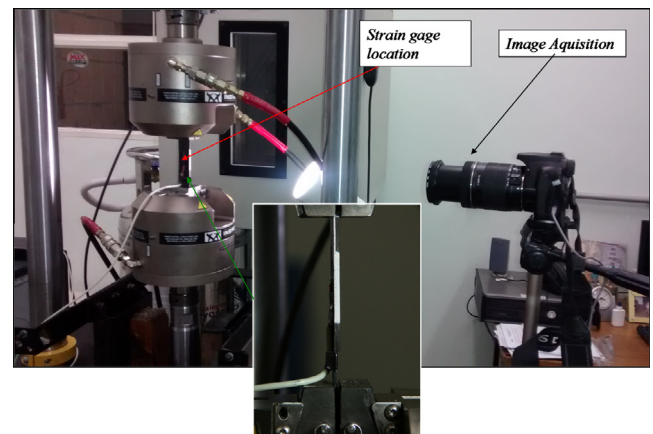

Fig. 4. Complete setup for axial test. (For interpretation of the references to color in this figure legend, the reader is referred to the web version of this article.)
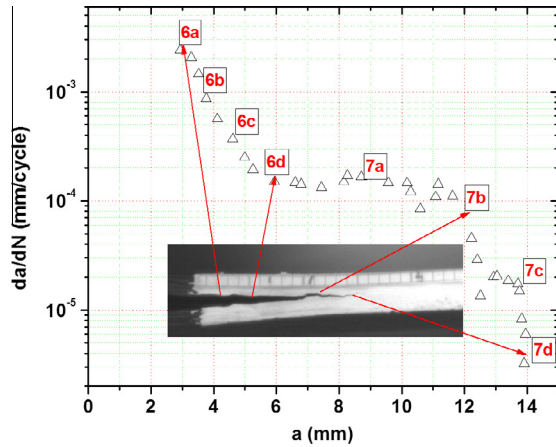
Fig. 5. Relative position of fracture surface in the crack growth rate curve – mode I. (For interpretation of the references to color in this figure legend, the reader is referred to the web version of this article.)

undefined inclination, as detailed in the orange box. Also this region is influenced by the weft region which location produces a local crack propagation that generates cusp patterns characteristically of interlaced fabrics [23]. The reason of having a local crack propagation is due to multiple crack propagation sites in each warp tow section that created this perpendicular and unstable one [24]. This point also forces the crack tip to back up due to an influence of crossover point [25] created by the fill/warp intersection [26] that consequently formed cusp patterns, as detailed in the green circle. Fig. 7b and c indicates also a similar angle to the previous analysis, Fig. 6c, which shows the direction of the global crack propagation. In Fig. 7d the crack reached a non linear region where the scarps have also an inclination different from θ that indicates a change in orientation of the global crack growth. This location could be considered a near threshold region.

3.2. Mode II – crack growth rate and fracture surface

Following the same analysis as conducted for mode I fatigue tests, the graphic for mode II did not exhibit non-linear behavior that divided the curve into two regions as exemplified in mode I, instead it presented a linear trend as shown in Fig. 8.

Two points are dislocated from the linear trend of the da/dN curve in blue circle, which could be related to the difficult task of following the crack increment from the specimens' edges and combined with the fact that the crack in mode II is constantly closed which makes the measurement not as clear as in mode I. This situation was also observed in static tests by Shiino et al. [3].

As pointed out in some studies [3,27], mode II loading covers an area of damage that normally neglects the crossover sections and fibers at 90° (weft tow), as a result the crack propagated without interference, as observed in mode I. Fig. 10 illustrates these observations by take into account the fracture sections obtained from decreasing crack growth rate in which, for example, Fig. 10a corresponds to a fatigue crack growth rate of 2.0×10^{-3} mm/cycle that is labeled as 10a in Fig. 9.

According to work conducted in [11,12] that reports fracture surface in mode II, the fracture patterns that appear in static test are cusps which are similar to that one observed in Fig. 10a in fatigue test. However it differs from each other in the fracture phase where the tip of the cusp tend to curve toward the final load cycle direction or extract out from the matrix, the latter formed another pattern named here as "*rollers*" [28,29].

The rollers are fracture patterns that are produced due to the friction of the upper and lower beam of the ENF specimen that eventually will be detached from the fracture surface [23,28].

Fig. 11a–c shows the fracture surfaces that correspond to decreasing crack growth rate that is located in Fig. 8. The roller as described in the last discussion is shown in the orange box in Fig. 11a, which is more geometrically defined for the first loading cycles (high da/dN) as compared with the ones shown in Fig. 11b and c. These fractures evidently exhibit the mechanism
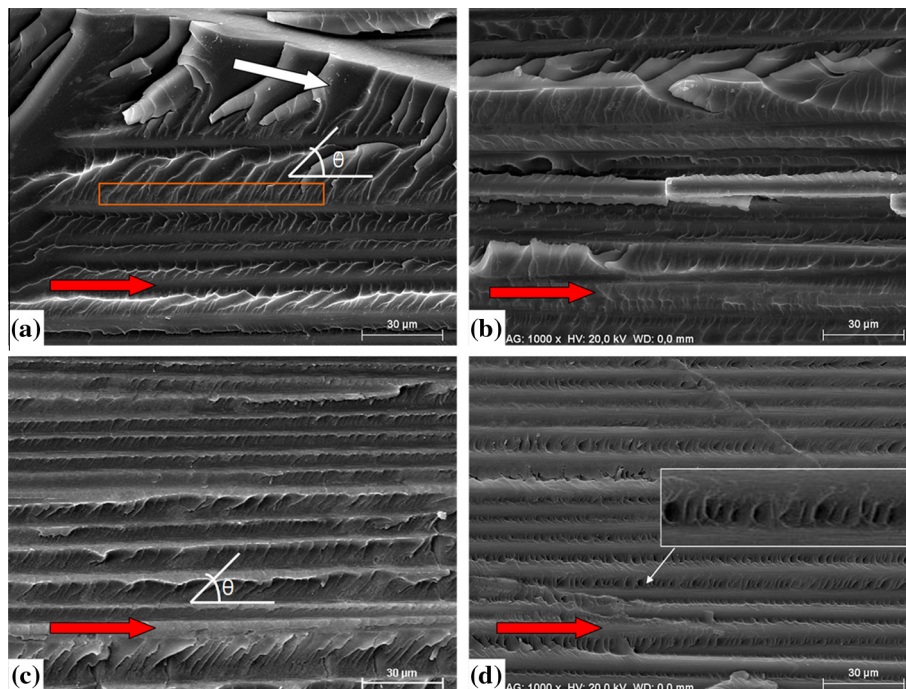

Fig. 6. Fracture surface for decreasing crack growth rate – first region. (For interpretation of the references to color in this figure legend, the reader is referred to the web version of this article.)
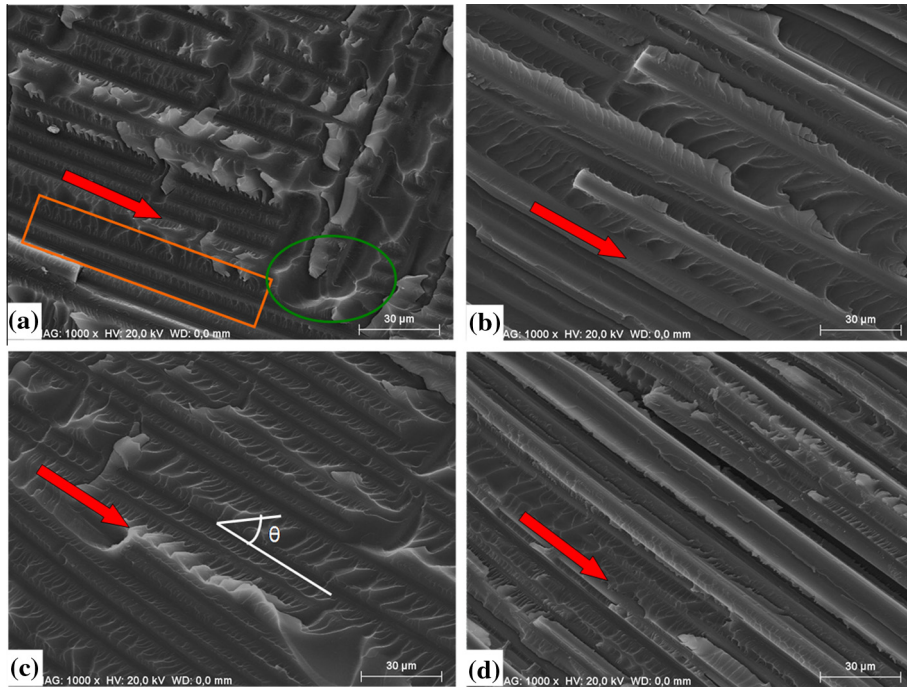
Fig. 7. Fracture surface for decreasing crack growth rate – second region. (For interpretation of the references to color in this figure legend, the reader is referred to the web version of this article.)
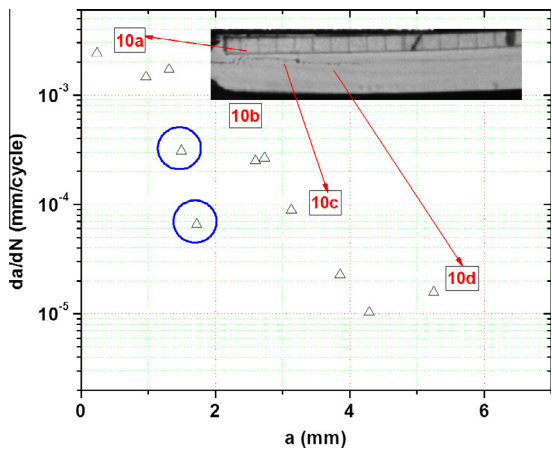

Fig. 8. Relative position of fracture surface in the crack growth rate curve – mode II. (For interpretation of the references to color in this figure legend, the reader is referred to the web version of this article.)

of shear loadings that preserved the aspect of fracture that enable the correlation of decreasing crack growth rate.

The direct consequence of decreasing value of crack growth rate is the enhanced grinding effect of constant movement of both faces of the specimens that produces a smooth surface, as far as we move from a region of critical energy (point 10a) to a threshold region (point 10d). The appearance of fracture surfaces in Fig. 10a–d qualitatively indicates this trend. It is worth mentioning that the degree of debris [30] also increased as the crack growth rate decreased.

3.3. Axial mode or mixed mode – crack growth rate and fracture surface

For axial mode of loading the crack initiated with minimum crack length for slow crack growth rate (*da/dN*) and it progressively increased with time and ended up with a value of high crack growth rate as seen in Fig. 12. In this mode of propagation, more scatter was observed in comparison to the pure modes which is caused by unstable propagation throughout the crack length,
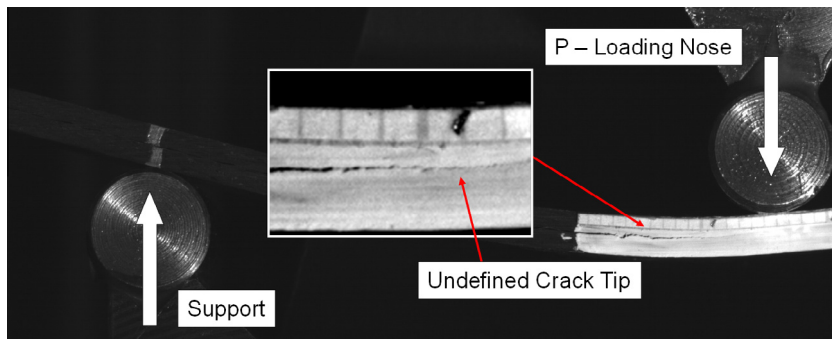

Fig. 9. Measurement of crack tip in mode II. (For interpretation of the references to color in this figure legend, the reader is referred to the web version of this article.)
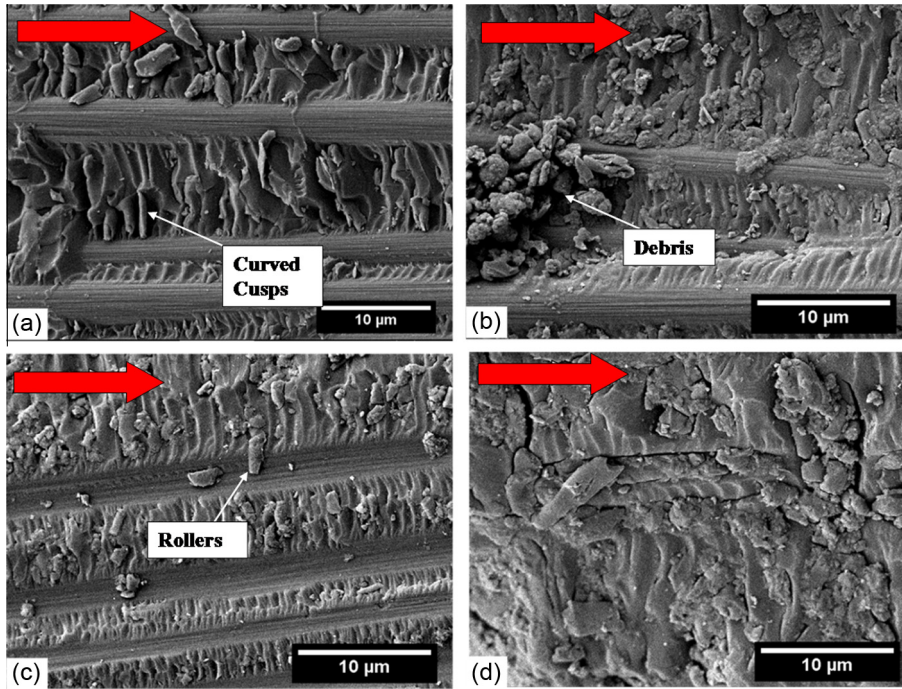
Fig. 10. Fracture surface for decreasing crack growth rate – mode II. (For interpretation of the references to color in this figure legend, the reader is referred to the web version of this article.)
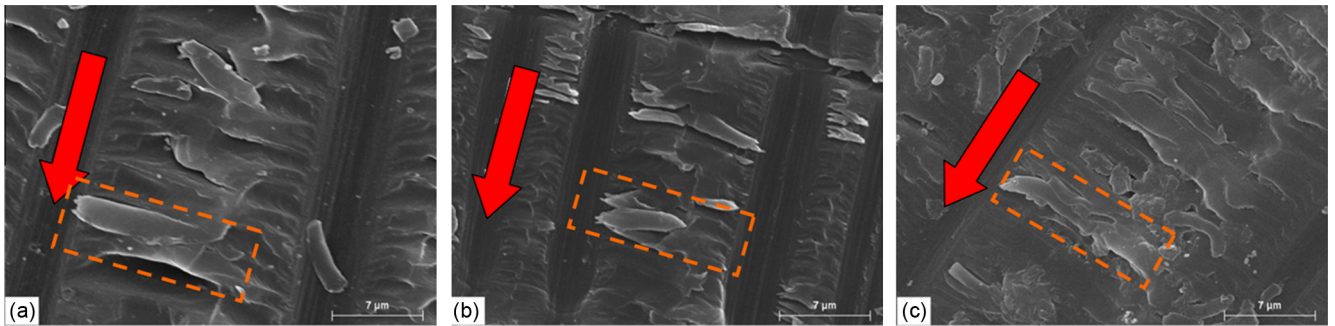

Fig. 11. Fracture patterns of fatigue test in mode II. (For interpretation of the references to color in this figure legend, the reader is referred to the web version of this article.)
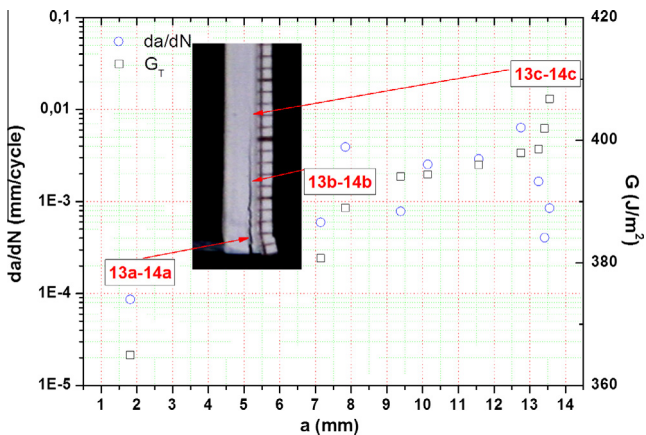

Fig. 12. Relative position of fracture surface in the crack growth rate curve – axial mode of loading. (For interpretation of the references to color in this figure legend, the reader is referred to the web version of this article.)

where the gap between points 9a–10a and 9b–10b in Fig. 12 presented this transition. The labels 13a–14a refer to fractures in Figs. 13a and 14a, respectively.

For this analysis the fracture surface of axial mode of loading is divided into lap section (interrupted ply) and strap section (continuous ply). Fig. 13a–c shows the lap sections which predominantly exhibit river markings (yellow boxes) that subsequently converged into scarps (red boxes). There was no clear relationship between crack growth rate with the aspect of the fracture surfaces, if we compare Fig. 13a with c which have the same space between the fibers. According to Svensson and Gilchrist an apparent increase in the fracture deformation would be an indication of increase in mode II of loading [31] What it was expected to see in the fracture surfaces is the characteristic feature of fracture toughness observed for high force values (critical values – G_c).

An aspect for considering these fractures (lap section) from axial mode is the similarity with pure mode I fracture surfaces. However, pure mode I shows sharper tip on the top of the scarps and also indicates the global crack propagation direction, where the axial mode indicates scarps perpendicular to the propagation direction and with a rounded tip.
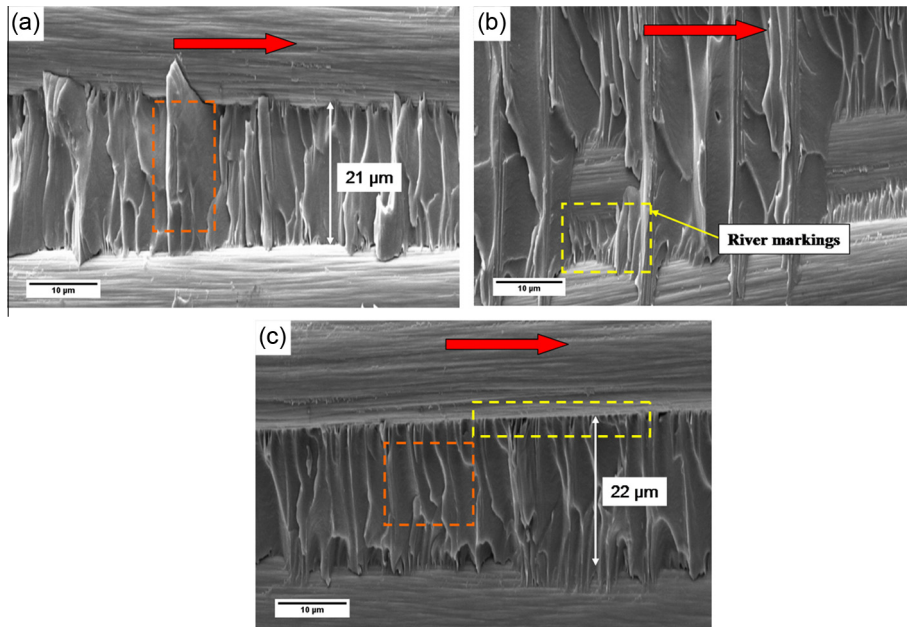
Fig. 13. Fracture surface for increasing crack growth rate for lap section – axial mode. (For interpretation of the references to color in this figure legend, the reader is referred to the web version of this article.)

Fig. 14. Fracture surface for increasing crack growth rate for strap section – axial mode. (For interpretation of the references to color in this figure legend, the reader is referred to the web version of this article.)
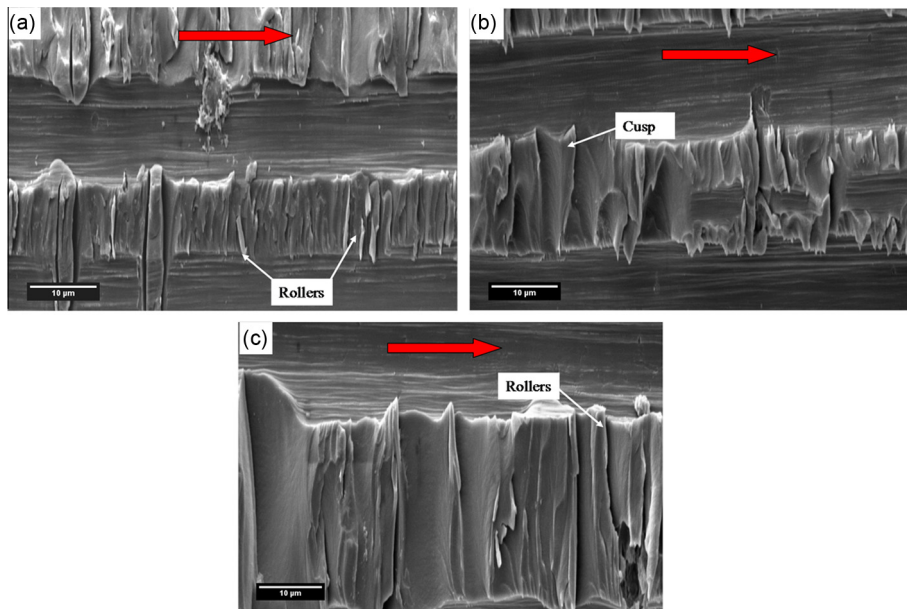
Based on the analysis of the lap section, one could conclude that the driving force in this mode of propagation is the mode I as the patterns suggest exactly this. However the matching surfaces of lap section, designated as strap section, show that the patterns have direct relationship with pure mode II crack propagation, illustrated by the comparison of Figs. 10 and 11 with images from Fig. 14. The rollers tend to appear in the CLS specimens, however less defined than in pure mode II. From the fractographic investigation it was also difficult to find a pattern that show evidence of the amplitude loading action.

These analyses show a partition of the crack tip into to very distinct mode of propagation that eventually interacts with each other as the evidence of rounded scarps instead of sharp ones that appear in pure mode I. If we consider that each half of the CLS specimen controls the crack propagation, it is intuitive to say that 50% of each mode controls the crack in axial loading as the fracture patterns are very distinguishable, or it can be said that G_I is equal to G_{II}.

The results of the fractures show some differences in values of G_I/G_{II} ratio from analytical solution results [6], as shown in Eq. (3), which is between 0.2 and 0.5. However the constant ratio of G_I/G_{II} from analytical solution as the crack length increases agrees with the fracture surfaces showed here. Other sources from the literature [22,32] also show that there is more contribution of mode II than mode I.

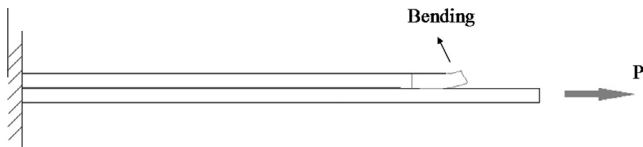$$G_1 = \frac{M_I^2}{2b^2}\left(\frac{1}{(EI)_1} - \frac{1}{(EI)_2}\right)$$

(3)

Fig. 15. Development of bending in the lap section.

where M_I is the flexure moment in the lap section, I the inertia moment, b the beam width and the subscript 1 is related to lap and 2 for strap section.

The solution of Eq. (3) does not take into account the anisotropic nature of the 5HS composite material interface, which may explain this difference. As it was observed in pure mode I the crossover section influenced the crack path. In addition to this, it can be attributed to the bending moment that is comparable to peeling load in the lap section, which increases mode I contribution, as exemplified in Fig. 15.

4. Conclusions and final remarks

In this research paper the authors showed the importance of conducting fractographic investigation based on well developed studies on fracture surfaces on pure modes of propagation to complement some results from analytical closed form solutions. This study illustrates that the two forms of analyses may present some discrepancy due to the material behavior.

Despite that the fracture from axial mode indicates that $G_I = G_{II}$, further quantitative analysis on the fracture is necessary to investigate if the strain energy intensity in each surface is evenly divided.

Moreover, the state of stress near the crack tip of CLS specimen seems to have a non-interactive loading modes I with II propagation behavior as it enables identifying the individual pure delamination modes that drive the crack. This discussion also emphasizes the constant ratio of G_I/G_{II} independent of the crack growth rate.

References

[1] Nishikawa Y, Okubo K, Fuji T, Kawabe K. Fatigue crack constrain in plain-woven CFRP using newly-developed spread tows. Int J Fatigue 2006;28:1248–53.
[2] Hansen U. Damage development in woven fabric composites during tension–tension fatigue. J Compos Mater 1999;7:614–39.
[3] Shiino MY, Alderliesten RC, Donadon MV, Voorwald HJC, Cioffi MOH. Applicability of standard delamination tests (double cantilever beam and end notch flexure) for 5HS fabric-reinforced composites en weft-dominated surface. J Compos Mater. http://dx.doi.org/10.1177/0021998314549821.
[4] Alif N, Carlsson LA, Boogh L. The effect of weave pattern and crack propagation direction on mode I delamination resistance of woven and carbon composites. Composites Part B 1998;28B:603–11.
[5] Shiino MY, Alderliesten RC, Pitanga MY, Cioffi MOH. Fatigue crack growth rate in mode I of a carbon fiber 5HS weave composite laminate via RTM. Adv Mater Res 2014;891–892:172–7.
[6] Johnson WS. Stress analysis of the cracked-lap-shear specimen: an ASTM round-robin. ASTM Int 1987;15:303–24.
[7] Lai Y-H, Rakestraw MD, Dillard DA. The cracked lap shear specimen revisited – a closed form solution. Int J Solid Struct 1996;12:1725–43.
[8] Reddy AD, Rehfield LW, Weinstein F, Armanios EA. Interlaminar fracture process in resin matrix composites under static and fatigue loading. Composite materials: testing and design (Eight conference); 1988. p. 340–55.
[9] Fortson BH, Armanios EA. Quantitative fractography of cracked lap shear composite specimen. Fract M Eng Mater: Comp Met 1993;2:205–17.
[10] Gilchrist MD, Svensson N. A fractographic analysis of delamination within multidirectional carbon/epoxy laminates. Compos Sci Technol 1995;55: 197–207.
[11] Greenhalgh ES, Rogers C, Robinson P. Fractographic observations on delamination growth and the subsequent migration through the laminate. Compos Sci Technol 2009;69:2345–51.
[12] Purslow D. Matrix fractography of fibre-reinforced epoxy composite. Composites 1986;17:289–303.
[13] Gilchrist MD, Kinloch AJ, Matthews FL. Mechanical performance of carbon-fibre and glass-fibre-reinforced epoxy I-beams: II. Fractographic failure observations. Compos Sci Technol 1996;56:1031–45.
[14] Mollón V, Bonhomme J, Viña J, Argüelles A, Fernández-Cantelli. Influence of the principal tensile stresses on the delamination fracture mechanisms and their associated morphology for different loading modes in carbon/epoxy composites. Composites Part B 2012;43:1676–80.
[15] Hein LR, Campos KA, Caltabiano PCRO, Kostov KG. A brief discussion about image quality and SEM methods for quantitative fractography of polymer composites. Scanning 2013;35:196–204.
[16] Rhee KY, Chi CH. Determination of fracture toughness, G_C of graphite/epoxy composites from a cracked lap shear (CLS) specimen. J Compos Mater 2001;35:77–93.
[17] Rhee KY. Characterization of delamination behavior of unidirectional graphite/ PEEK laminates using cracked lap shear specimens. Compos Struct 1994;29:379–82.
[18] Feret V, Ghiasi H, Hubert P. Effect of fibre volume fraction on mixed-mode fracture of a fabric carbono/epoxy composite. Appl Compos Mater 2013;20:415–29.
[19] Charalambous G, Allegri G, Lander JK, Hallett SR. A cut ply specimen for the mixed-mode fracture toughness and fatigue characterization of FRPs. Composites Part A 2015;74:77–87.
[20] Standard a. D5528-01 2001. Standard test method for Mode I interlaminar fracture toughness of unidirectional fiber-reinforced polymer matrix composites. Am Soc Test Mater 2014:1–13. http://dx.doi.org/10.1520/D5528-13.2.
[21] ÓBrien TK, Jonhston WM, Toland GJ. Mode II interlaminar fracture toughness and fatigue characterization of a graphite epoxy composite material. NASA, NASA/TM-2010-216838.
[22] Mangalgiri PD, Johnson WS. Preliminary design of cracked-lap shear specimen thickness for determination of interlaminar fracture toughness. J Compos Technol Res 1986;2:58–60.
[23] Greenhalgh E. Failure analysis and fractography of polymer composites. CRC Press; 2009.
[24] Kim J-K, Sham M-L. Impact and delamination failure of woven-fabric composites. Compos Sci Technol 2000;60:745–61.
[25] Nishikawa Y, Okubo K, Fuji T, Kawabe K. Fatigue crack constrain in plain-woven CFRP using newly-developed spread tows. Int J Fatigue 2006;28:1248–53.
[26] Kumar MS, Ambresha M, Panbarasu K, Kishore N, Ranganath VR. A comparative study of failure in aerospace grade unidirectional and bidirectional woven CFRP composites under four-point bend fatigue loads. Materialwissenschaft and Werkstofftechnik 2011;20:644–51.
[27] Moura MFSF, Campilho RDSG, Goncalvez JPM. Pure mode II fracture characterization of composite bonded joints. Int J Solids Struct 2009;46: 1589–95.
[28] Al-Khudairi O, Hadavinia H, Waggott A, Lewis E, Little C. Characterizing mode I/mode II fatigue delamination growth in unidirectional fibre reinforced polymer laminates. Mater Design 2015;66:93–102.
[29] Blanco N, Gamstedt EK, Asp LE, Costa J. Mixed-mode delamination growth in carbon-fibre composite laminates under cyclic loading. Int J Solid Struct 2004;41:4219–35.
[30] Kenane M, Benmedakhene S, Azari Z. Fracture study of unidirectional glass/ epoxy laminate under different mode of loading. Fatigue Fract Eng Mater Struct 2010;33:284–93.
[31] Svensson N, Gichrist MD. Mixed mode delamination of multidirectional carbon fiber/epoxy laminates. Mech Compos Mater Struct 1998;5:291–307.
[32] Ramkumar RL, Whitcomb JD. Characterization of mode I and mixed-mode delamination growth in T300/5208 graphite/epoxy. Am Soc Test Mater 1985:315–35.